INTERNATIONAL JOURNAL OF CONSERVATION SCIENCE
ISSN: 2067-533X Volume 15, Issue 4, 2024: 1731-1754 www.ijcs.ro
DOI: 10.36868/IJCS.2024.04.10

NUMERICAL THERMAL-MECHANICAL ANALYSIS OF PASSIVELY PROTECTED STEEL STRUCTURES UNDER FIRE CONDITIONS

Kseniya YURKOVA[1], Maciej MAJOR[1], Izabela MAJOR[1], Joanna GONDRO[2], Damian JOŃCZYK[1,*]

[1] Czestochowa University of Technology, Faculty of Civil Engineering, Department of Civil Engineering, 3 Akademicka, Czestochowa 42-218, Poland
[2] Czestochowa University of Technology, Faculty of Production Engineering and Materials Technology, Department of Physics, al. Armii Krajowej 19, 42-200 Częstochowa, Poland

Abstract

Structures made of materials with high thermal conductivity quickly reach critical temperature in fire situation. The drastic reduction of plasticity occurring due to this may contribute to rapid destruction of the element. The necessity of protecting steel structures in fire conditions is currently included in building standards and is becoming one of the fundamental issues of designing steel structures. Numerical simulations are an important tool for analyzing the behavior and selection of protection measures of structures in fire conditions. The article presents a numerical analysis of mechanical and thermal behavior of steel beams in fire conditions using different methods of fire insulation. The analysis included a beam with concrete casing, with casing made of thermal insulation boards, with fire protection spraying and compared with a beam without fire protection. The dependence of strength properties of construction materials on thermal temperature was taken into account. Four-sided thermal interactions in the beam cross-section were assumed, taking into account heat flow by convection and radiation. The course of fire overtime was modelled in accordance with the standard curve according to ISO 834. The results of thermal analysis were presented in the form of temperature distribution for the analysed models and the influence of temperature increase under fire conditions on the change in the load-bearing capacity of beams (in the stress-strain state) was shown.

Keywords*: Thermal-mechanical analysis; Fire safety; Steel; Concrete, Strength*

Introduction

Steel structures are characterized by low resistance to high temperatures. Rapid temperature increases occur, among others, in fire conditions and according to standard curves [1] can reach up to 1200°C. A steel structure not protected against fire is quickly destroyed by very high temperatures due to a significant reduction in the strength properties of steel. Due to the high thermal conductivity of steel and the exceptional and sometimes difficult to predict fire conditions, the risk of failure increases after just 10 minutes from the start of the fire. The need to protect the life and health of people and valuable equipment requires the use of appropriate fire protection [1-7]. The aim is to extend the time in which it will be possible to evacuate people from the facility. According to standards [3], the strength properties of structural steels decrease after reaching a temperature of 400°C, while changes in the Young's modulus value

* Corresponding author: damian.jonczyk@pcz.pl

occur already at 150-200°C. Load-bearing structures made of wood, ordinary concrete and full ceramics behave in a similar way. Only for selected wall materials, including for aerated concrete and silicates, significant strength gains can be observed in the temperature range of 250÷650°C [8].

First and foremost, it is important to protect the steel frame elements. In addition to active protection, i.e. fire alarms, passive fire protection is used, which consists in isolating the steel frame elements from zones exposed to fire. It is also necessary to protect individual load-bearing elements against premature occurrence of the critical temperature in steel, i.e. the temperature under the influence of which the destruction of the structural element occurs.

The design of steel structures in terms of their fire resistance [9, 10] is possible based on fire tests, tabulated data or calculation methods. However, in general, the following should be taken into account:

- the proper course of fire over time;
- changes in temperatures in the tested structure during the fire (so-called thermal impacts);
- the mechanical response of the tested structure, which is the effect of both thermal impacts and their influence on changes in material properties, as well as direct mechanical impacts.

In the literature, you can find manuals published by companies dealing with fire protection for the design of steel structures with regard to fire conditions [11-13], which can be helpful in analyzing the necessary solutions to be applied. When considering a fire protection system, the method of insulating the steel profile should be taken into account [14-17]. The profile surfaces can be directly covered with an insulating material applied by spraying. Alternatively, the profile is covered with special insulating concrete. An effective and popular way to obtain the required fire resistance class by the protected element is to use special fire protection boards. Most often, gypsum plasterboards or gypsum fiber boards and mineral wool linings are used for this purpose, which are attached to the structure with mechanical connectors or by gluing with thermo-resistant mortars [18].

Due to the low resistance of steel structures to high temperatures, research is commonly conducted on various aspects of fire resistance of steel structures. One of the most important aspects of fire design is to design a structure so that during a fire the time during which the structure operates without failure is sufficient for the evacuation of people. In the event of further fire development, a building disaster is often inevitable. An extensive review of building failures related to fire was made in [19] while the methods of assessing the degree of destruction of the structure after the fire in [20]. In the article [19] attention was drawn to the usefulness of numerical calculations due to the possibility of analyzing multi-storey buildings in a spatial manner. Currently, the use of programs based on FEM is often used because this approach allows for taking into account many geometric and material factors. There is a lack of such experimental studies due to safety reasons and due to the very high costs of such studies. For the above reasons, numerical studies in the analysis of structural elements are often used in many ways for various structural elements [21-24]. The most commonly used in building structures is ordinary steel and in order to provide adequate fire protection, appropriate safeguards must be made. A comprehensive review of research on high-strength steel operating in fire conditions can be found in [25]. The authors of [25] draw attention to the need to adapt normative provisions to the properties of high-strength steel. Passive fire protection is directly related to the properties of structural elements. Many studies can be found on various forms of passive fire protection. Elements made of cement [26] and gypsum [27] materials are often used as fire protection materials. Elements made of the aforementioned materials are often made in the form of a casing and tested in this way. An additional protection is to leave a gap between the structural element and the casing. Such a solution was tested in [28]. An unusual form of fire protection was presented in [29], showing that wood significantly improves the temperature

distribution in the steel cross-section by acting as an insulator. An important aspect in the use of structural elements with fire protection is the situation of destruction of the protection and the impact of this destruction on the further operation of the element during a fire. In [30], a steel connection with partially destroyed fire protection was numerically analyzed. Potential destruction of the casing leads to a rapid increase in the temperature of the structural element. A special situation that can lead to potential destruction of the casing is the possibility of seismic loads, which was analyzed in [31]. In the literature, one can also find works presenting less typical cases of fire protection, such as: protection of pipelines [32], protection using GFRP glass fiber reinforced cement boards [33], fire protection in Arctic conditions [34]. Among the presented studies, there are many analyses of individual solutions, but there are no comparative analyses of different passive protections, which would allow for estimating which protections are the most effective.

The aim of this work is to:

- determine the temperature distributions during a fire in a steel beam that is not insulated and is fire-insulated in different ways;
- determine the mechanical response of fire-protected models of a beam loaded to the ultimate limit state (the beginning of the plastic phase) in fire conditions;
- determining how an exceptional fire situation affects the load-bearing capacity, ultimate limit state and serviceability of a fire-protected steel structure.

Materials and Methods

General assumptions for the issue being solved

Designing fire insulation of a steel structure is usually based on three key factors [2]: the fire resistance class specified in the regulations, the critical temperature and the shape solidity factor.

Information on the fire resistance period, which can be found in local building regulations, is given for a specific building height, as well as its intended use. It is necessary to determine the appropriate temperature (critical) that a given section will not withstand. The shape solidity factor, i.e. the ratio of the heated surface area to the volume of the element, is used to assess the fire resistance of the building in a similar way based on a separate thermal-static-strength analysis [8]. In this article, the effect of insulation thickness on the load-bearing capacity of a steel beam was explicitly analyzed using numerical simulations.

The numerical analysis was performed using the standard fire curve. The heating of the elements can be modeled using the analytical method given in standards [1, 3], in which the temperature increase depends on the thermal effects (expressed as net heat fluxes), thermal properties of steel and the exposure index.

The results of fire resistance tests are expressed as a function of the time the structure operates without failure. It is assumed that the safety limit is at a temperature of 450°C [15]. Beyond this point, the loss of strength progresses rapidly.

When considering the fire protection system, three methods of insulating the steel profile were taken into account (Figure 3, Table 1):

- covering with sprayed insulating material;
- encasing the profile with special insulating concrete;
- encasing with insulating boards, mounted in a box.

Sprayed coatings [16, 35] are 10 to 50 mm thick. They allow for a fire resistance period of 30 to 120 minutes. They are made of materials based on cement and gypsum containing mineral fibres, expanded vermiculite and/or other lightweight aggregates or fillers. The minimum spray thickness for open-section profiles is selected depending on the mass factor and the required fire resistance classes R15 to R180 [4, 35].

The PROMASPRAY P300 fire-protective mortar based on vermiculite and gypsum [36] was used for numerical simulation.

The next choice for numerical analysis was the insulation system made of gypsum plasterboards, because this system is currently the most commonly used fire protection due to the widespread use of gypsum plasterboards. In the article, gypsum plasterboards with a thickness of 12.5 and 20.0mm and a density of 900kg/m^3 are used as an example of fire protection in the form of fire protection boards.

According to the standards, the thickness of gypsum plasterboards should be selected for the required fire resistance depending on the mass factor of the steel section. In the article, the thickness of the plasterboards is selected so that the temperature of the steel beam protected against fire does not reach the critical temperature in the numerical calculation. For comparison with the mentioned fire protection systems, a numerical simulation was also carried out for the variant with a concrete casing, which is a less common type of protection. For this purpose, two types of concrete were assumed: ordinary concrete of strength class C55/67 (in the calculations it acts as an insulating and structural material) and lightweight concrete with an expanded clay aggregate (in the calculations it acts only as an insulating material).

Theoretical basis

The total net heat flux value h_{net} [W/m^2] determines the thermal effects on the surface of the element. This value is determined by taking into account the heat flow by convection and radiation [1, 9]:

$$h_{net} = h_{net,c} + h_{net,r} \tag{1}$$

where: $h_{net,c}$ – convective heat flux, $h_{net,r}$ – radiative heat flux.

Convective heat flux is assumed according to the dependence [1, 9]:

$$h_{net,c} = \alpha_c\left(\theta_g - \theta_m\right) \tag{2}$$

where: α_c – convective heat transfer coefficient [W/m^2], θ_g – gas temperature in the vicinity of the element exposed to fire [°C], θ_m – surface temperature of the element [°C].

Net radiative heat flux per unit area is determined according to the formula [1, 9]:

$$h_{net,r} = \Phi\varepsilon_m\varepsilon_f\sigma[(\theta_r + 273)^4 - (\theta_m + 273)^4] \tag{3}$$

where: Φ – configuration factor (Φ = 1.0), ε_m – emissivity of the element surface (for steel [37] $\varepsilon_{s,m}$ = 0.8, for concrete $\varepsilon_{b,m}$ = 0.94, for plasterboard $\varepsilon_{g,m}$ = 0.9, for fire protection spray $\varepsilon_{n,m}$ = 0.80), ε_f – fire emissivity (ε_f = 1.0), σ – Stefan-Boltzmann constant = 5.67·10^{-8} W/m^2·K), θ_r – effective radiation temperature of the fire environment [°C].

For elements engulfed in fire on all sides, the radiation temperature θ_r can be assumed as the gas temperature θ_g in the element's surroundings. The surface temperature θ_m of the element is obtained as a result of thermal analysis of the element, while the gas temperature θ_g is determined based on the standard temperature-time curve.

To determine the course of fire over time in numerical calculations, the standard curve according to ISO 834 was adopted. It describes the gas temperature as a function of fire duration for a fully developed fire without a cooling phase and is the most commonly used fire scenario.

The standard temperature-time function is defined by the formula [1, 6]:

$$\theta_g = 20 + 345 \cdot \log_{10}(8t + 1) \tag{4}$$

where: t – time [min].

The heat transfer coefficient by convection is: α_c = 25 [W/m^2·K] in the case of using the standard curve.

Material models in thermal analysis

The numerical analysis was carried out in two forms:

• Thermal analysis (calculation of the course of changes in the temperature distribution in the beam): the net heat flow value at the edges of the element exposed to fire is used as the fire load);
• Coupled thermal-mechanical analysis (determination of the mechanical response of the beam to thermal effects); the mechanical load (external forces) is used as the load at stage 1 and the temperature distribution in the test element, changing with time, at stage 2).

The aim of the thermal analysis is to determine the relationship between the temperature in the element and the time it takes to reach this temperature (both in the case of elements not covered with fireproof insulation and those covered). By determining the temperature in the steel element during the considered time t of the fire duration, its degree of effort in the fire can be assessed.

The aim of the thermal-mechanical analysis is to determine the relationship between the strength characteristics of the element and the fire duration.

Thermal analysis is the first stage of the calculation of a structure in fire conditions, which is linked to the mechanical analysis. The principle of energy conservation in thermal analysis is taken into account by using the Fourier conductivity equation:

$$\rho c \frac{\partial T}{\partial t} = \mathrm{div}(\lambda \mathrm{grad} T) \tag{5}$$

where: λ – thermal conductivity [W/m K], c – specific heat [J/kg K], ρ – density [kg/m^3].

The reliability of calculations in thermal analysis depends on the correct determination of the basic thermal properties of concrete, primarily thermal conductivity λ and volumetric specific heat (ρ_c).

According to the standard PN-EN 1993-1-2 [3], the values of specific heat $c_p(\theta)$ [J/kg K] for steel in a dry state can be determined based on the following relationship:

$$c_s(\theta) = 425 + 7.73 \cdot 10^{-1}\theta - 1.69 \cdot 10^{-3}\theta^2 + 2.22 \cdot 10^{-6}\theta^3 \text{ for } 20 \le \theta \le 600°\text{C}, \tag{6}$$

$$c_s(\theta) = 666 + \frac{13200}{738-\theta} \text{ for } 600 < \theta \le 735°\text{C}, \tag{7}$$

$$c_s(\theta) = 545 + \frac{17820}{\theta-731} \text{ for } 735 < \theta \le 900°\text{C}, \tag{8}$$

$$c_s(\theta) = 650 \text{ dla } 900 \text{ for } 900 < \theta \le 1200°\text{C}. \tag{9}$$

For steel, the thermal conductivity in the same temperature range can be assumed according to the standard PN-EN 1993-1-2 [3] as follows:

$$\lambda_s(\theta) = 54 - 3.33 \cdot 10^{-2}\theta \text{ for } 20 \le \theta \le 800°\text{C}, \tag{10}$$

$$\lambda_s(\theta) = 27.3 \text{ for } 800 < \theta \le 1200°\text{C}. \tag{11}$$

According to the standard PN-EN 1992-1-2 [38], the values of specific heat $c_b(\theta)$ [J/kg K] for concrete in a dry state can be determined based on the following relationship:

$$c_b(\theta) = 900 \text{ for } 20 \le \theta \le 100°\text{C}, \tag{12}$$

$$c_b(\theta) = 800 + \theta \text{ for } 100 < \theta \le 200°\text{C}, \tag{13}$$

$$c_b(\theta) = 1000 + \frac{\theta-200}{2} \text{ for } 200 < \theta \le 400°\text{C}, \tag{14}$$

$$c_b(\theta) = 1100 \text{ for } 400 < \theta \le 1200°\text{C}. \tag{15}$$

The change in density with increasing temperature, which is caused by water loss, can be determined according to [38] as follows:

$$\rho_b(\theta) = \rho(20°\text{C}) \text{ for } 20 \le \theta \le 115°\text{C}, \tag{16}$$

$$\rho_b(\theta) = \rho(20°\text{C}) \cdot (1 - 0.02(\theta - 115)/85) \text{ for } 115 < \theta \le 200°\text{C}, \tag{17}$$

$$\rho_b(\theta) = \rho(20°\text{C}) \cdot (0.98 - 0.03(\theta - 200)/200) \text{ for } 200 < \theta \le 400°\text{C}, \tag{18}$$

$$\rho_b(\theta) = \rho(20°\text{C}) \cdot (0.95 - 0.07(\theta - 400)/800) \text{ for } 400 < \theta \le 1200°\text{C}. \tag{19}$$

For high-strength concretes, the thermal conductivity in the same temperature range can be assumed according to PN-EN 1992-1-2 [38] as follows:

$$\lambda_b(\theta) = 1.8 - 0.7(\theta - 20)/180 \text{ for } 20 \le \theta \le 200°C, \quad (20)$$

$$\lambda_b(\theta) = 1.1 - 0.3(\theta - 200)/800 \text{ for } 200 < \theta \le 1000°C, \quad (21)$$

$$\lambda_b(\theta) = 0.8 \text{ for } 1000 < \theta \le 1200°C. \quad (22)$$

For lightweight concrete, thermal conductivity is lower than for normal concrete. In the entire temperature range, the values of this parameter for lightweight concrete are 10-20% lower. Summary of thermal properties of all materials used has been presented in Table 1.

Table 1. Thermal material parameters of steel, concrete, plasterboard, fire retardant spray [39].

Material parameter	20°C	200°C	300°C	600°C	1200°C
Specific heat of steel, c_s [J/kg K]	460	470	480	490	520
Thermal conductivity of steel, k_s [W/mK]	15	17	18	22	30
Specific heat of concrete, c_b [J/kg K]	900	1000	1050	1200	1300
Thermal conductivity of concrete, k_b [W/mK]	1.8	1.1	1.0635	0.95	0.8
Specific heat of plasterboard panels, $c_{g\text{-}k}$ [J/kg K]	1000	1000	1000	1000	1000
Thermal conductivity of plasterboard panels, $k_{g\text{-}k}$ [W/mK]	0.25	0.25	0.25	0.25	0.25
Specific heat of spray insulation, c_p [J/kg K]	1011	1012	1022	1035	1050
Thermal conductivity of spray insulation, k_p [W/mK]	0.0237	0.02512	0.0307	0.036	0.05

Reduction factors for the stress-strain relationship for carbon steel at elevated temperatures are given in Table 2. Temperature-dependent mechanical properties of the materials are given in Tables 3 - 8.

Table 2. Reduction factors for elastic and strength material parameters of steel [3, 8]

Material parameter	20°C	200°C	300°C	600°C	1200°C
Reduction factor of the modulus of elasticity of steel	1	0.9	0.8	0.31	0.045
Reduction factor of the effective yield strength of steel	1	1	1	0.47	0.04
Reduction factor of the proportional limit of steel	1	0.807	0.613	0.18	0.025

Table 3. Elastic and strength material parameters of steel [3, 5]

Material parameter	20°C	200°C	300°C	600°C	1200°C
Modulus of elasticity of steel, $E_{s,\theta}$ [GPa]	200	180	160	62	9
Poisson's ratio of steel, v_s [-]	0.3	0.3	0.3	0.3	0.3
Effective yield strength of steel, $f_{y,\theta}$ [MPa]	235	235	235	110.5	9.4
Strain at yield strength, $\varepsilon_{y,\theta}$ [-]	0.02	0.02	0.02	0.02	0.02
Proportional limit of steel, $f_{p,\theta}$ [MPa]	235	189.6	144.1	42.3	5.9
Strain at proportional limit, $\varepsilon_{p,\theta}$ [-]	0.001175	0.001054	0.0009	0.000682	0.000653

The strength and deformation properties of carbon steels at elevated temperatures are obtained according to the formulas [3], provided that the heating rate is within the range of 2÷50 K/min [3]:

$$\sigma = E_{s,\theta}\varepsilon, \text{ for } \varepsilon \le \varepsilon_{\mathrm{p},\theta}, \quad (23)$$

$$\sigma = \mathrm{f}_{\mathrm{p},\theta} - c + (b/a)\left[a^2 - \left(\varepsilon_{\mathrm{y},\theta} - \varepsilon\right)^2\right]^{0.5}, \text{ for } \varepsilon_{\mathrm{p},\theta} \le \varepsilon \le \varepsilon_{\mathrm{y},\theta}, \quad (24)$$

$$\sigma = \mathrm{f}_{\mathrm{y},\theta}, \text{ for } \varepsilon_{\mathrm{y},\theta} \le \varepsilon \le \varepsilon_{\mathrm{t},\theta}, \quad (25)$$

where:

$$a^2 = \left(\varepsilon_{\mathrm{y},\theta} - \varepsilon_{\mathrm{p},\theta}\right)\left(\varepsilon_{\mathrm{y},\theta} - \varepsilon_{\mathrm{p},\theta} + c/E_{s,\theta}\right), \quad (26)$$

$$b^2 = c\left(\varepsilon_{\mathrm{y},\theta} - \varepsilon_{\mathrm{p},\theta}\right)E_{s,\theta} + c^2, \quad (27)$$

$$c = \frac{\left(\mathrm{f}_{\mathrm{y},\theta} - \mathrm{f}_{p,\theta}\right)^2}{\left(\varepsilon_{\mathrm{y},\theta} - \varepsilon_{\mathrm{p},\theta}\right)E_{s,\theta} - 2\left(\mathrm{f}_{\mathrm{y},\theta} - \mathrm{f}_{\mathrm{p},\theta}\right)}, \quad (28)$$

$$\varepsilon_{\mathrm{p},\theta} = \mathrm{f}_{p,\theta}/E_{s,\theta}, \; \varepsilon_{\mathrm{y},\theta} = 0.02, \; \varepsilon_{\mathrm{t},\theta} = 0.15. \quad (29)$$

Thermal properties of the materials are given in Table 1. Stress-strain graphs for carbon steel at elevated temperatures are given in Figure 1.

As the temperature increases, many processes occur in concrete resulting in significant changes in its mechanical properties [38, 40-32]. The behavior of concrete depends significantly on its composition, but generally, after exceeding the temperature level of approx. 300°C, there is a noticeable decrease in strength for ordinary concrete and with a further increase in temperature above 600°C, concrete becomes practically unsuitable as a construction material due to a large - even over 50% - reduction in compressive strength. For high-strength concretes, significant reductions in compressive strength of the order of 50% can occur already at lower temperatures at the level of 300-400°C [43].

In the design of concrete structures subjected to high temperatures, the σ–ε relationship for concrete in compression must be determined as a function of temperature. The strength and deformation properties of concrete under uniaxial compression at elevated temperature are defined according to the standard [38] by two basic parameters: $f_{c,\theta}$ – the compressive strength of concrete at temperature θ and $\varepsilon_{c1,\theta}$ – the deformation corresponding to the value of $f_{c,\theta}$.

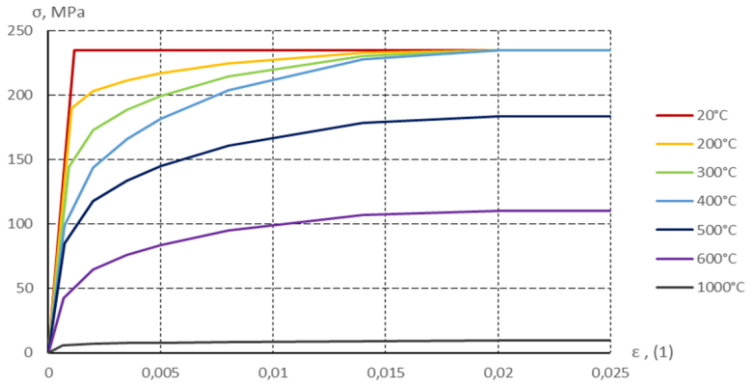

Fig. 1. Stress-strain relationships for carbon steel at elevated temperatures

The strength and deformation properties of concrete at elevated temperatures are obtained (Fig. 2), according to the formulas [38]:

$$\sigma = \frac{3\varepsilon\, f_{c,\theta}}{\varepsilon_{c1,\theta}\left(2+\left(\frac{\varepsilon}{\varepsilon_{c1,\theta}}\right)^3\right)} \text{ for } \varepsilon \le \varepsilon_{c1,\theta}, \tag{30}$$

descending curve (linear and nonlinear models) for $\varepsilon_{c1,\theta} \le \varepsilon \le \varepsilon_{cu,\theta}$,

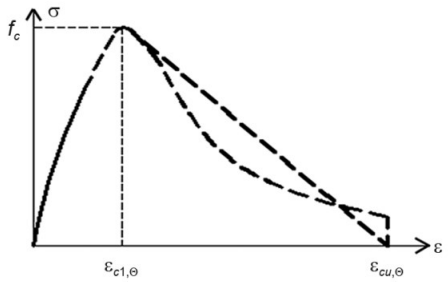

Fig. 2. Stress-strain relationships for carbon steel at elevated temperatures [35]

The values of the basic parameters of the relationship σ – ε for high-strength concrete in compression as a function of temperature according to EN 1992-1-2 [38] are presented in

Table 4. The tensile strength of concrete can be assumed in accordance with the standard PN-EN 1992-1-2 [38] as follows:

$$f_{ck,t}(\theta) = f_{ck,t} \text{ for } 20 \le \theta \le 100°C, \quad (31)$$

$$f_{ck,t}(\theta) = (1 - (\theta - 100)/500) f_{ck,t} \text{ for } 100 < \theta \le 600°C. \quad (32)$$

Table 4. Elastic and strength material parameters of concrete [38]

Temperature	$f_{c,\theta}/f_{c,k}$	$f_{t,\theta}/f_{c,k}$	$f_{b,\theta}/f_{c,k}$	$\varepsilon_{c1,\theta}$	$\varepsilon_{cu,\theta}$	$E_{c,\theta}/E_{c,2\theta}$
20	1.0	1.0	1.0	0.0025	0.02	1.0
200	0.9	0.8	0.9	0.0055	0.025	0.8
300	0.85	0.6	0.85	0.007	0.0275	0.63
600	0.45	0.1	0.45	0.025	0.035	0.18
1000	0.04	0.01	0.04	0.025	0.045	0.02

For beams with concrete casing, calculations were performed in two options: M-W model taking into account strengthening and weakening (MW model with HSD2) for high-strength concrete (HSC) class C55/67 and lightweight concrete with expanded clay aggregate (K). HSC concrete is considered in numerical calculations as a construction material. Lightweight concrete, on the other hand, is considered in numerical calculations only as a thermal insulation material, just like gypsum board and material for spray coating. Parameters given in Table 5 and Table 6.

Table 5. Elastic and strength material parameters of concrete [38]

Material parameter	Value
Initial Young's modulus, $E_{b,\theta}$ [MPa]	38280
Initial Poisson coefficient, v_b [-]	0.2
Tensile strength, $f_{t,\theta}$ [MPa]	3.99
Compressive strength, $f_{c,\theta}$ [MPa]	56.4
Biaxial compressive strength, $f_{b,\theta} = 1.15\, f_{c,\theta}$ [MPa]	64.86
Fracture energy, G_{ft} [N/m]	151

Table 6. Elastic and strength material parameters of concrete at elevated temperatures [21, 30, 31]

Material parameter	20°C	200°C	300°C	600°C	1200°C
Initial Young's moduli $E_{b,\theta}$ [MPa]	38280	30624	24116.4	6890.4	765.6
Tensile strength $f_{t,\theta}$ [MPa]	3.99	3.19	2.39	0.4	0.04
Compressive strength $f_{c,\theta}$ [MPa]	56.4	50.76	47.94	25.38	2.25
Biaxial compressive strength $f_{b,\theta}$ [MPa]	64.86	58.37	55.13	29.19	2.59

The inelastic parameters of the material models are listed in the tables: a) Table 7 for the case of an elastic-plastic material with reinforcement (dependent on temperature) b) Table 8 for an elastic-plastic material with reinforcement and weakening (MW model with HSD2) defined in the ANSYS program [42, 44, 45]. The graphs representing the stress-strain relationships for concrete at elevated temperatures are given in Figure 3.

Table 7. Plastic material parameters of concrete (List of material constants used to determine the parameters of the M-W model for HSD2 strengthening/weakening) [42, 44, 45]

Material parameter	Value
Plastic strain at uniaxial compressive strength, κ_{cm}	0.0053
Plastic strain at transition from power law to exponential softening, κ_{cu}	0.00175
Relative stress at start of nonlinear hardening, Ω_{ci}	0.33
Residual relative stress at κ_{cu}, Ω_{ci}	0.85
Residual compressive relative stress, Ω_{cr}	0.2
Residual tensile relative stress, Ω_{tr}	0.1

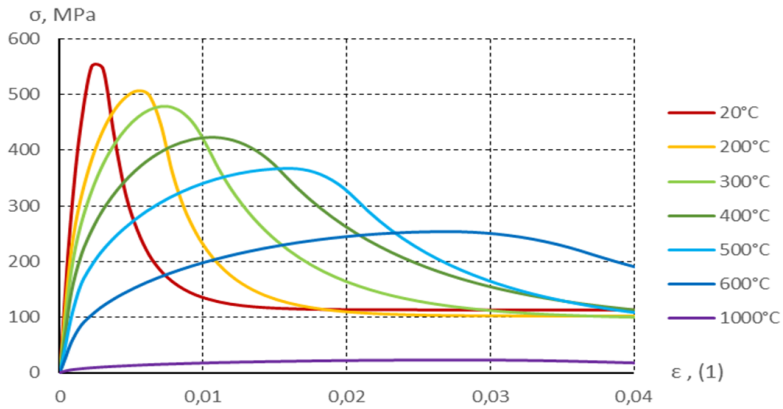

Fig. 3. Stress-strain relationships for concrete at elevated temperatures

Table 8. Plastic material parameters of concrete at elevated temperatures [42, 44, 45]

Material parameter	20°C	200°C	300°C	600°C	1000°C
Plastic strain at uniaxial compressive strength, κ_{cm}	0.00053	0.000281	0.000717	0.0023	0.0022
Plastic strain at transition from power law to exponential softening, κ_{cu}	0.00175	0.00154	0.00256	0.00467	0.00580
Relative stress at start of nonlinear hardening, Ω_{ci}	0.33	0.33	0.33	0.25	0.16

The contact between the steel beam and the concrete of the structure was assumed to be rigid. The interactions between the beam and the support were taken into account by introducing a flexible contact model, i.e. allowing for slippage of the contact surfaces with respect to each other with a friction coefficient of $\mu = 0.2$.

Material models in mechanical calculations

The mechanical model takes into account the nonlinear behavior of structural materials. Material nonlinearity occurs due to the nonlinear relationship between stress and strain, stress is a nonlinear function of strain.

A model of an elastic-plastic material was assumed in which stress is a nonlinear function of strain:

$$\dot{\sigma} = C^e : \dot{\varepsilon}^e \tag{33}$$

where: σ is the stress tensor, C^e is the elastic stiffness tensor, ε^e is the elastic strain tensor.

In the case of nonlinear materials, the elastic strains in equation (34) have the form:

$$\dot{\varepsilon} = \dot{\varepsilon}^e + \dot{\varepsilon}^p + \dot{\varepsilon}^{th}, \qquad \dot{\varepsilon}^p = \dot{\gamma}\frac{\partial Q}{\partial \sigma}, \tag{34}$$

where: ε^p is the plastic strain tensor, ε^{th} is the thermal strain tensor.

The theory of plasticity defines mathematical relationships characterizing the elastic-plastic response of materials. These are: the plasticity criterion, the flow rule and the hardening rule. The plasticity criterion determines the stress level at which plasticization begins, the flow rule determines the direction of plastic deformation and the hardening rule describes the change in the yield surface during plastic hardening.

In mechanical calculations, in accordance with the recommendations of standards [3, 38], material models defined in the ANSYS program [44] were used:

- In the case of steel, a multilinear elastic-plastic model with reinforcement (Multilinear Isotropic Hardening) was adopted.
- In the case of concrete, an elastic-plastic model with the Menetrey-Willam surface with reinforcement/weakening in compression and tension, the HSD2 model, implemented in the ANSYS program and regularized by fracture energy [44, 45], was adopted.

Multilinear elastic-plastic model with reinforcement (Multilinear Isotropic Hardening).

During plastic deformation, isotropic hardening causes a uniform increase in the size of the yield surface and causes an increase in the yield strength. The plasticity criterion has the form:

$$F(\sigma) - \sigma_y(\xi) = 0 \tag{35}$$

where: $F(\sigma)$ is a scalar function of stress and $\sigma_y(\xi)$ is the yield stress, which evolves as a function of a set of internal material variables.

The von Mises yield criterion is assumed, which is commonly used in plasticity models for a wide range of materials. It is a good first approximation for metals, among others.
The von Mises yield criterion is:

$$f(\sigma, \sigma_y) = \sigma_e - \sigma_y = 0, \tag{36}$$

where: σ_e is the von Mises effective stress, also known as the von Mises equivalent stress,

$$\sigma_e = \sqrt{\frac{3}{2}}\left(\sigma : \sigma - \frac{1}{3} tr(\sigma)^2\right), \tag{37}$$

and σ_y is the yield stress and corresponds to the yield stress under uniaxial loading. Multilinear Isotropic Hardening behavior is described by a piecewise linear stress-total strain curve starting from the origin and defined by sets of positive stress and strain values, as shown in Figure 4 [22]

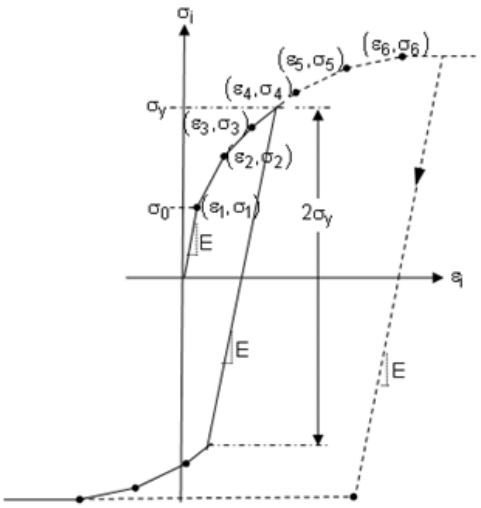

Fig. 4. Multilinear stress-strain curve

Menetrey–Willam elastoplastic model

The flow surface in the Menetrey–Willam (M-W) model [44, 45] is a function of the invariants and deviators of the stress tensor in the form

$$f_{MW} = \frac{c_2}{c_3}\left[\frac{\sqrt{2}}{\sqrt{3}} I_1 + r\rho\right] + \rho^2 - \frac{1}{c_3}, \rho = \sqrt{3J_2} \tag{38}$$

where: I_1 is the first invariant of the stress tensor, J_2 is the second invariant of the stress tensor deviator, r is a function of the stress deviator invariants and material parameters, c_2 and c_3 are quantities dependent on the hardening/weakening function in compression Ω_c and tension Ω_t and the material parameters

$$c_2 = \frac{1}{\sqrt{6}}\left[\frac{1}{\Omega_c f_c} - \frac{1}{\Omega_c f_b} + \frac{\Omega_c f_b - \Omega_{tc} f_t}{(\Omega_c f_c)^2}\right], \qquad c_3 = \frac{3}{2}\frac{1}{(\Omega_c f_c)^2} \tag{39}$$

$$r(\theta, e) = \frac{4(1-e^2)\cos^2\theta + (2e-1)^2}{2(1-e^2)\cos\theta + (2e-1)[4(1-e^2)\cos^2\theta + 5e^2 - 4e]^{0,5}} \tag{40}$$

$$e = \frac{1+\epsilon}{2-\epsilon}, \qquad \epsilon = \frac{\Omega_{tc} f_t}{\Omega_c f_b} \frac{(\Omega_c f_b)^2 - (\Omega_c f_c)^2}{(\Omega_c f_c)^2 - (\Omega_{tc} f_t)^2}, \qquad \Omega_{tc} = \begin{cases} \Omega_t \text{ for } \kappa_c \le \kappa_{cm} \\ \Omega_t \Omega_c \text{ for } \kappa_c > \kappa_{cm} \end{cases} \tag{41}$$

In equations (14), κ_c is the internal compression parameter, θ is the Lode angle (deviatoric angle), f_t is the uniaxial tensile strength, f_c is the compressive strength, f_b is the two-dimensional compressive strength. It is assumed that the flow rule in M-W is unrelated and defined by the relation (34) through the plastic potential $Q = Q_{MW}$ [44]

$$Q_{MW} = \rho^2 + B_g \rho + C_g \frac{I_1}{\sqrt{3}}, \tag{42}$$

$$B_g = \frac{2(\Omega_c f_c') \tan\psi - \sqrt{2}(\Omega_{tc} f_t)}{\sqrt{3\left(1 - \sqrt{2}\tan\psi\right)}}, \qquad C_g = \frac{B_g}{\sqrt{2}} + \frac{2(\Omega_{tc} f_t)}{\sqrt{3}}, \tag{43}$$

The strengthening and weakening in the M-W model are defined by the functions $\Omega_{\_c}$ and $\Omega_{\_t}$, which describe the material behavior in tension and compression (the functions depend on the internal parameters κ analyzed in the model during compression $\kappa = \kappa_c$ and tension $\kappa = \kappa_t$, [44]. The internal parameter κ is assumed to be the one-dimensional plastic strains under the influence of tension and compression. The strengthening/weakening function in compression $\Omega_{c,\kappa} = \kappa_c$

$$\Omega_c = \begin{cases} \Omega_{ci} + (1-\Omega_{ci}) \sqrt{2\frac{\kappa}{\kappa_{cm}} - \frac{\kappa^2}{\kappa_{cm}^2}}, & \kappa < \kappa_{cm}, \\ 1 - (1-\Omega_{cu}) \left(\frac{\kappa - \kappa_{cm}}{\kappa_{cu} - \kappa_{cm}}\right)^2, & \kappa_{cm} \le \kappa \le \kappa_{cu}, \\ \Omega_{cr} + (\Omega_{cu} - \Omega_{cr}) \exp\left(2\frac{\Omega_{cu} - 1}{\kappa_{cu} - \kappa_{cm}} \cdot \frac{\kappa - \kappa_{cu}}{\Omega_{cu} - \Omega_{cr}}\right), & \kappa_{cu} < \kappa, \end{cases} \tag{44}$$

Exponential tensile weakening function $\Omega_{t,\kappa} = \kappa_t$

$$\Omega_t = \exp\left(-\frac{\kappa}{a_t}\right), \qquad a_t = \frac{g_{ft}}{f_t}, \qquad g_{ft} = \max\left(\frac{G_{ft}}{L_i}, \frac{f_t^2}{E}\right) \tag{45}$$

where: L_i is the effective length of the element, E is the Young's modulus, G_{ft} is the fracture energy.

The significance of the parameters κ_{cm}, κ_{cu}, Ω_{cr}, Ω_{tr} characterizing the evolution of the strengthening/weakening function in compression and tension Ω_c and Ω_t is shown in Figure 5.

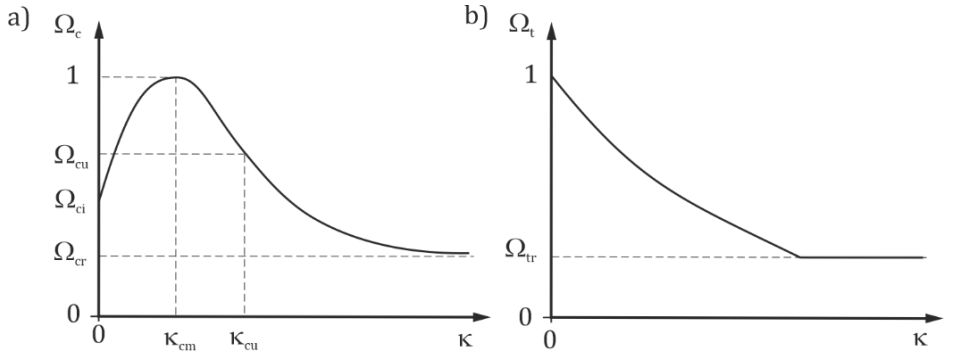

Fig. 5. Strengthening/weakening functions in compression Ω_c and tension Ω_t.

Numerical model

For the numerical analysis of the strength of steel structures in fire conditions, a freely supported beam, i.e. a beam with freedom of thermal deformations [40], was assumed as the test sample. Thermal deformations resulting from the action of elevated temperature are the result of thermal expansion of the material. In the case of a statically determinate beam (full

freedom of displacement of the element nodes), no additional internal forces are generated and the durability is determined only by the degree of reduction of the mechanical properties of the beam material. Therefore, the subject of the analysis is the fire durability of a steel beam, freely supported, uniformly loaded on the upper flange (simulation of the load from the floor slab), subjected to the action of high temperatures on all four sides (such boundary conditions were assumed as the most unfavourable from the point of view of the load-bearing capacity of the structure). For testing purposes, the beam has a span of 1 m and a cross-section of IPE 120 [46, 47] (h = 120mm, b = 64mm, A = 13.2cm^2, W_x = 53cm^3). The beam is made of S235 steel with strength parameters of f_y = 235MPa, E_s = 200GPa. Three different types of fire insulation were selected:

- concrete casing (in two options: HSC and expanded clay);
- gypsum board casing (in two options: 12.5 mm thick and 20mm thick);
- insulating sprayed fireproof coating.

According to the standards [1, 8], the basic goal of assessing fire durability is to determine the time in which the beam as a load-bearing element is able to transfer loads and will not be destroyed (fail). In other words, it is determining the critical temperature. It is also recommended [1, 8, 48] that the most unfavourable design effect of external load should not exceed the design load-bearing capacity of the element, reduced due to fire action. The load-bearing capacity, according to the recommendations of these standards, is determined at the level of characteristic strength (γ_M = 1.0), which means an additional safety reserve, due to the fact that fire conditions are an exceptional design situation. Therefore, the value of mechanical load in numerical calculations was selected in such a way that the normal stresses of the span cross-section reached the characteristic strength value of the beam material (the beginning of plastic deformation of the beam material). Through a series of test calculations of the beam for bending with protection against buckling, the load value was determined at the level of p = 1750kPa, which corresponds to

$$M_{max}=(1750\cdot 0.064)\cdot 1^2/8=14 \text{ kNm} > M_{pl}=235\cdot 10^3\cdot 53\cdot 10^{-6}=12.455 \text{ kNm}. \quad (46)$$

Each type of insulation covers the beam from four sides. The FEM models of the analyzed beam for two of the considered variants are shown on Fig. 6: a steel beam without fire protection (Fig. 6a and b) and a steel beam with concrete construction (Fig. 6c and d). Due to symmetry, half of the beam was assumed for calculations. Table 9 contains designations for beam models subjected to mechanical and thermal loads. Figure 7 shows cross-sections of the applied steel beam models with different types of fire protection.

FEM calculations were performed for test beams [44] loaded mechanically and thermally. Due to symmetry, half of the beam was used for calculations.

The eight-node Solid278 element was adopted as the finite element for thermal calculations and the Solid185 element for mechanical calculations, respectively. The contact between the beam and the support was considered via the Target 170 and Conta 174 contact elements [44].

Table 9. List of designations of steel beam models analyzed in the work in terms of fire resistance.

Material parameter	Model
Steel beam	B1
Steel beam with HSC concrete casing	B2_HSC
Steel beam with expanded clay concrete casing	B2_K
Steel beam with 12.5 mm thick plasterboard casing	B3_12.5
Steel beam with 20 mm thick plasterboard casing	B3_20
Steel beam with insulating spray coating	B4

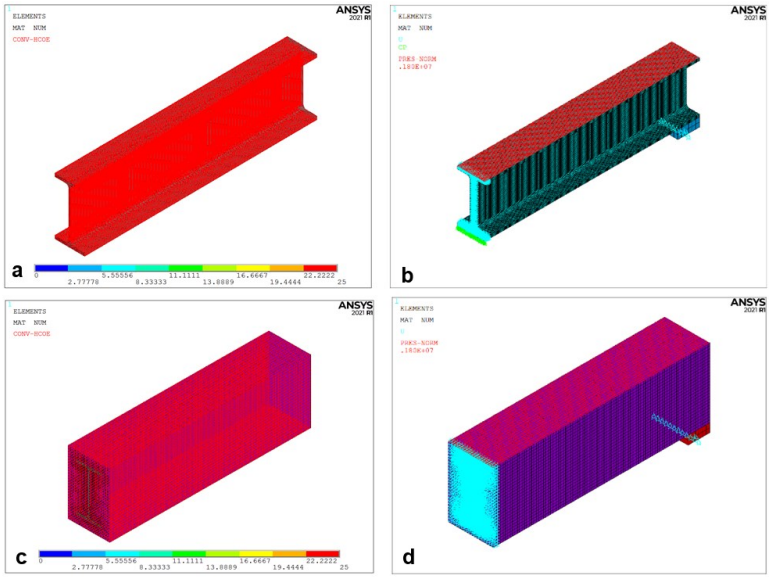

Fig. 6. Computer model of the analyzed element: a) steel beam without fire protection (thermal FEM model); b) steel beam without fire protection (mechanical FEM model); c) Steel beam with concrete construction (thermal FEM model); d) Steel beam with concrete construction (mechanical FEM model)

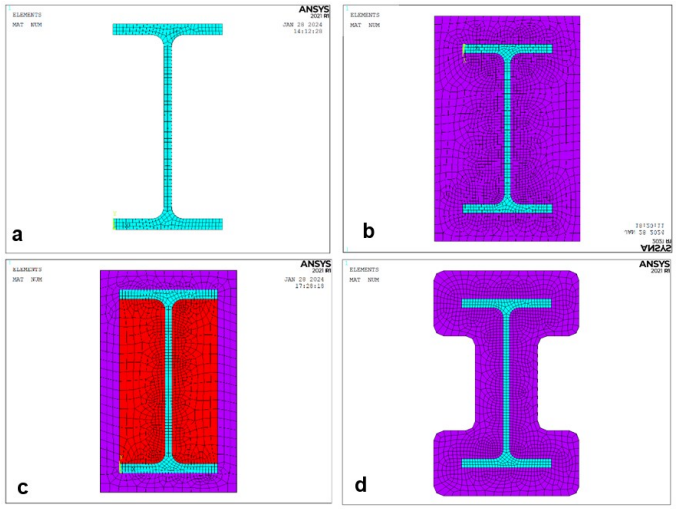

Fig. 7. The models of beam cross-sections under mechanical and thermal loading analyzed in the paper: a) steel beam without fire protection; b) steel beam with concrete casing; c) steel beam with plasterboard casing; d) steel beam with sprayed insulation coating

Thermal expansion coefficients were assumed for construction materials: $\alpha_{t,s}$=0.000012 for steel, $\alpha_{t,b}$ = 0.00001 for HSC concrete. Thermal expansion of gypsum plasterboards expanded clay concrete and fire protective spray for beam with fire protection has no effect on mechanical calculations due to the exclusively insulating function of the cladding. Densities: ρ_s = 7850kg/m^3 for steel, ρ_b = 2300kg/m^3 (20°C) for concrete, $\rho_{g\text{-}k}$ = 900kg/m^3 for plaster board, ρ_p = 150kg/m^3 for spray coating and for ρ_{air} = 1.25kg/m^3 air.

Results and discussion

Figures 8-10 show the temperature distributions at the appropriate time of the fire: 200, 600, 900 and 3600s. The temperature distributions in all protected beams are more favourable than in the case of the unprotected beam.

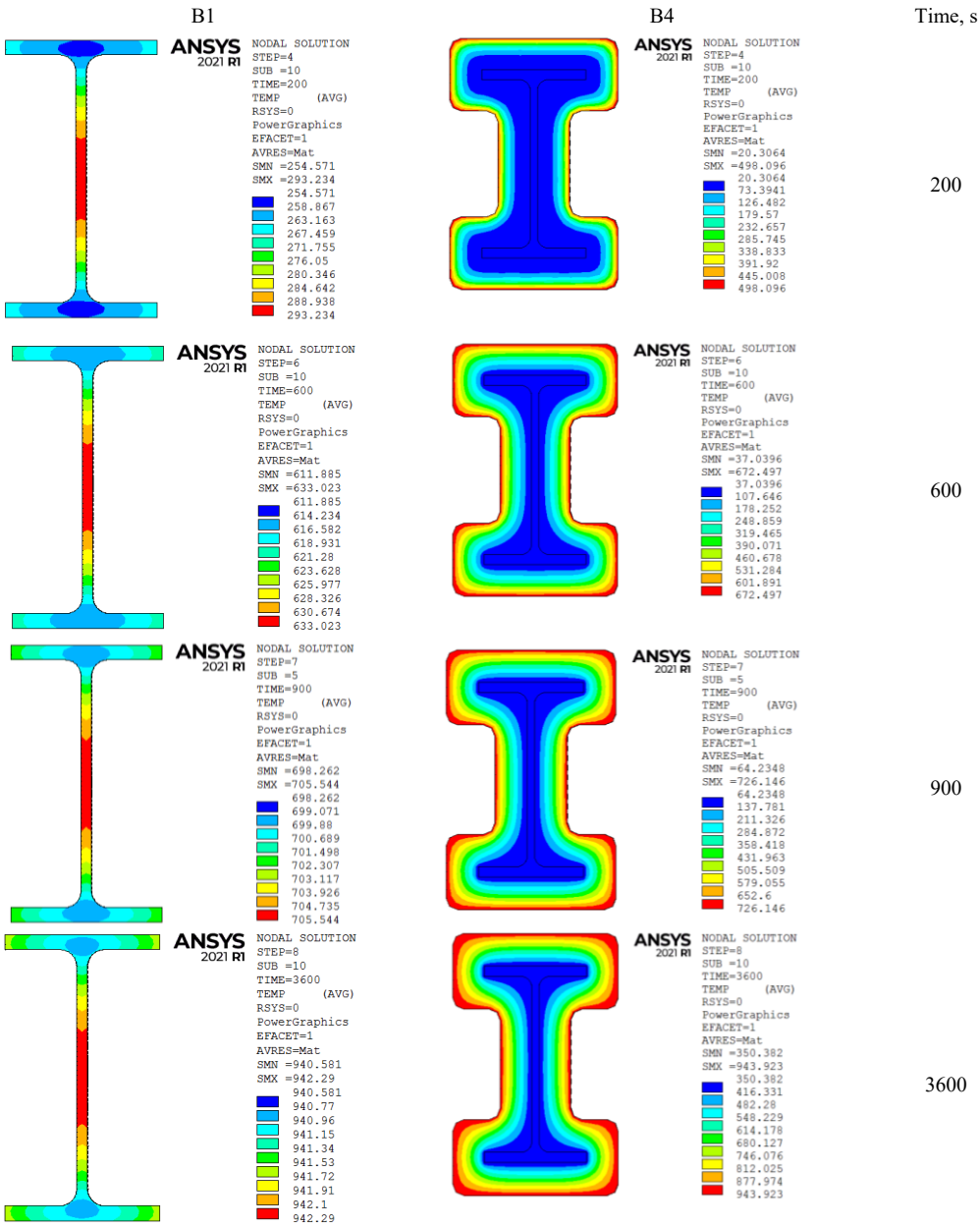

Fig. 8. Temperature distribution for models B1, B4 for time t = 3.33, 10, 15, 60min

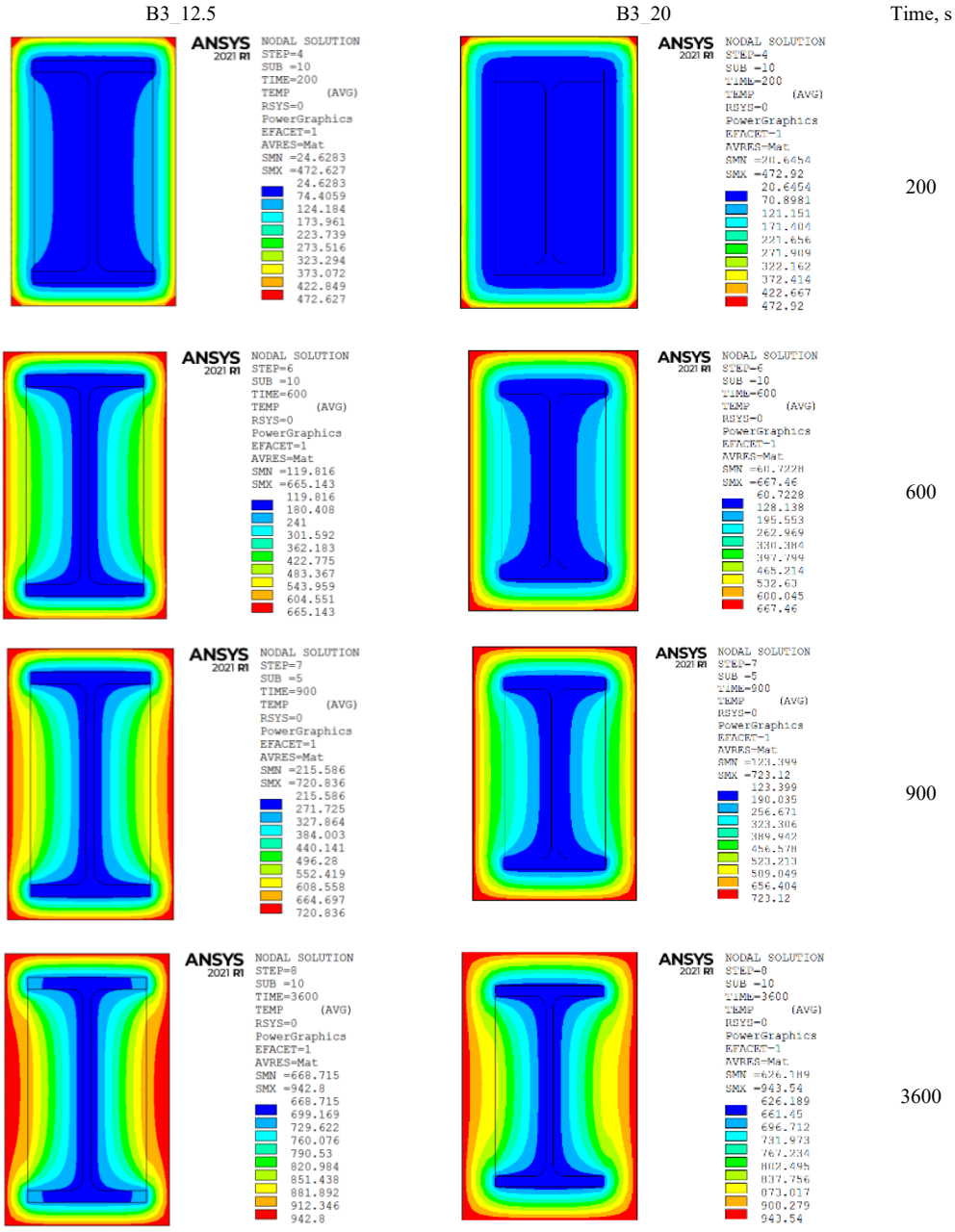

Fig. 9. Temperature distribution for models B3_12.5 and B3 for time t = 3.33, 10, 15, 60min

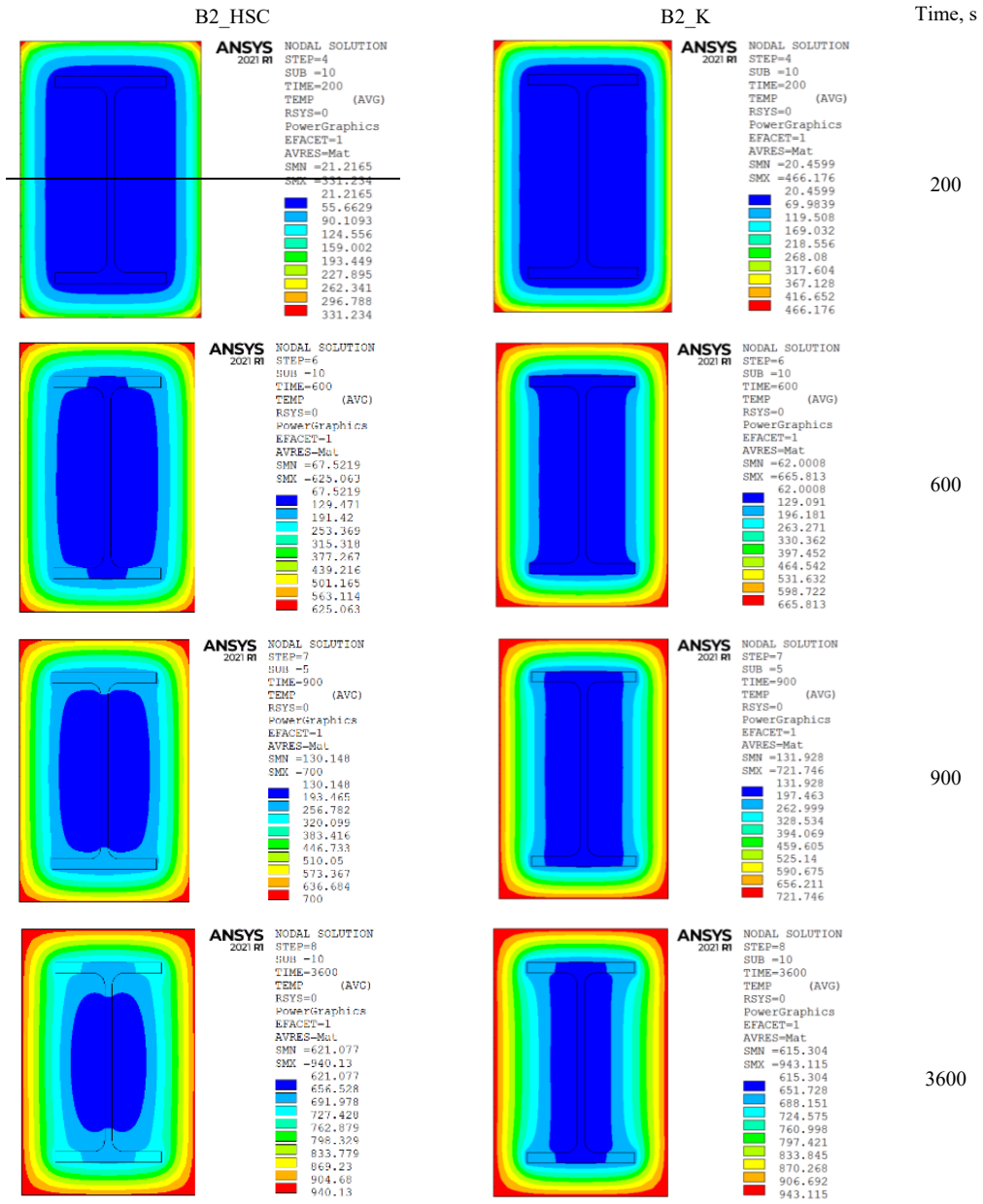

Fig. 10. Temperature distribution for models B2_HSC and B2_K for time t = 3.33, 10, 15, 60min

The temperature in the middle of the steel cross-section in the case of protected elements increases the fastest when encased with plasterboards. The slowest temperature increase in the steel cross-section can be observed when protected using fire protection spray. Figure 11 shows a graph of the dependence of the deflection of the middle span as a function of time for all beam calculation models. The slowest increase in deflection during exposure to fire is shown by the spray-protected element.

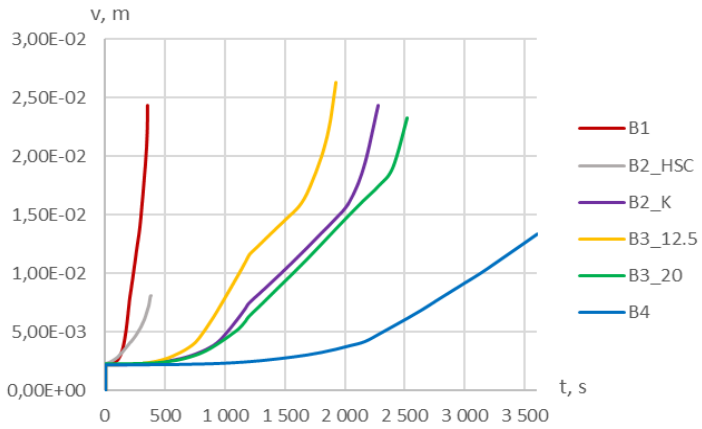

Fig. 11. Midspan displacement (maximum beam deflection) as a function of time for models B1 – B4

Protection in the form of an enclosure made of plasterboards and expanded clay concrete shows a similar nature of deflections. In mechanical terms, the solution with an ordinary concrete enclosure is the most disadvantageous due to the rapid increase in beam deflection over time and the rapid loss of load-bearing capacity. The deflection values at the moment of beam destruction, together with the given temperatures and the time of destruction from the start of the fire, are presented in Table 10.

Table 10. Summary of results for fire resistance of the analyzed beam models

Model	Deadweight loss time, s	Maximum temperature of steel beam, °C	Deflection at destruction cm
B1	352	463	2.43
B2_HSC	381	34	0.8
B2_K	2280	451	2.44
B3_12.5	1920	452	2.63
B3_20	2520	430	2.32
B4	3600*	356*	1.34*

* the beam with fire protection spray did not achieve the loss of fire load-bearing capacity for the time set as the maximum calculation time (60 minutes). The table shows the corresponding results for the time of 3600 s.

Figure 12 shows the temperature distribution at the moment of loss of load-bearing capacity (corresponds to the moment at which the uncontrolled increase in beam deflection begins).

Figure 13 shows the distribution of principal stresses for beam models loaded mechanically (until the yield point of the beam material is reached) and thermally (until the moment of loss of fire load-bearing capacity).

Figure 14 shows a graphical representation of the main plastic strains in the B2_HSC beam at the time of fire initiation and at time t = 380s for the M-W model with strengthening and weakening in compression and tension. Figure 15 shows the changes that occur in the stress distribution in steel (Fig. 15a) and concrete (Fig. 15b) in the beam protected by concrete.

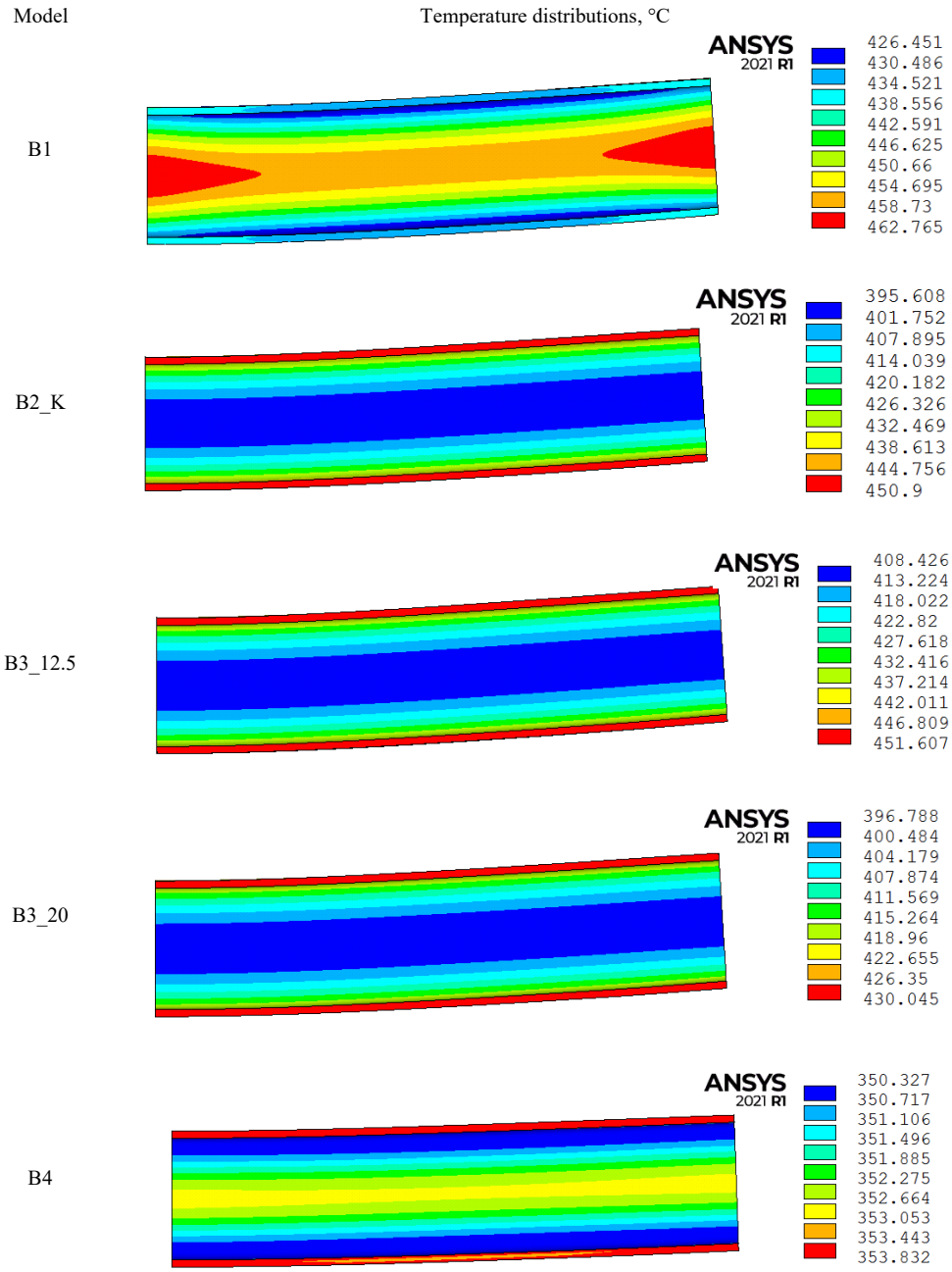

Fig. 12. Temperature distribution at the moment of reaching the loss of fire load-bearing capacity

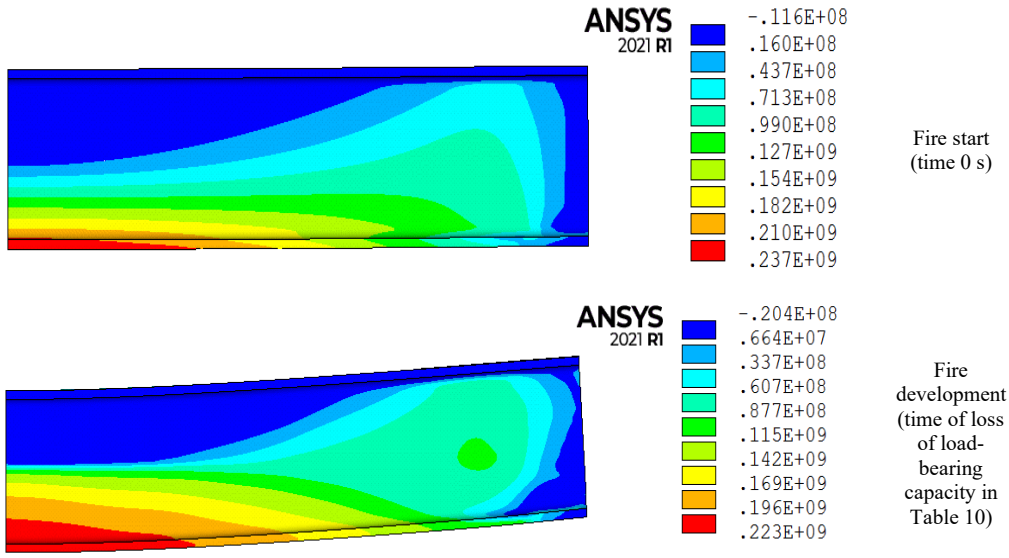

Fig. 13. Map of principal stresses at the moment of reaching the yield strength of the beam material and the moment of losing the fire load-bearing capacity

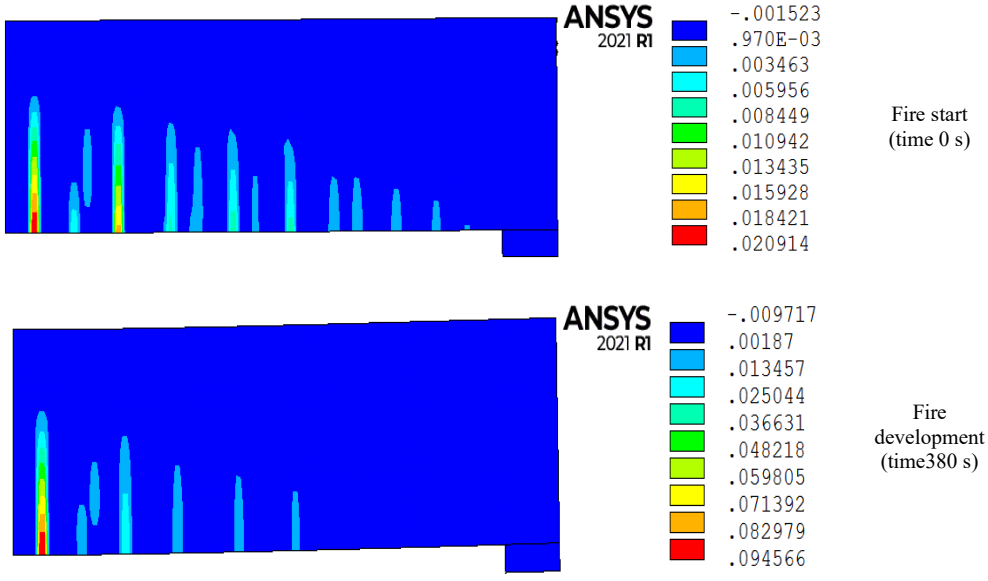

Fig. 14. Longitudinal strain maps for the B2_HSC model

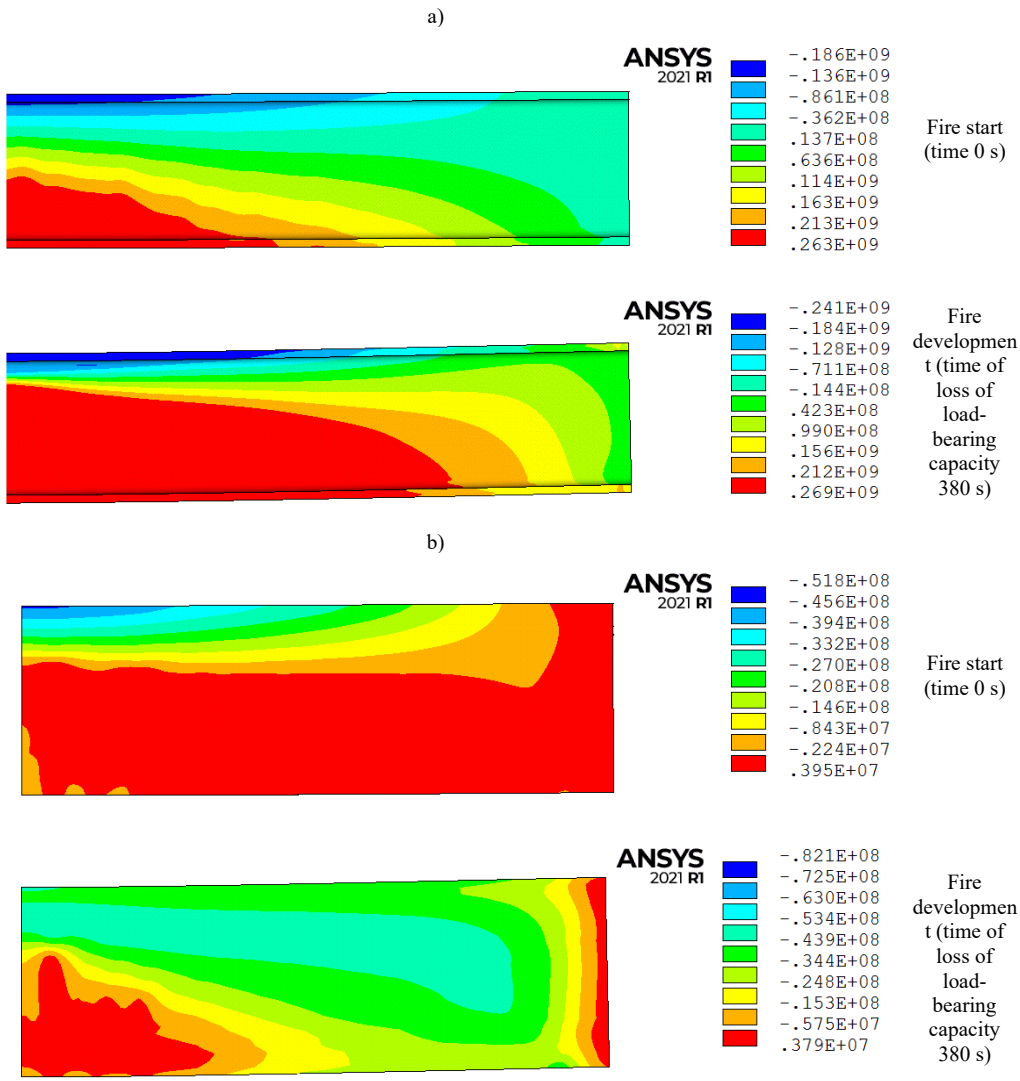

Fig. 15. Longitudinal stress maps for the B2_HSC model (Pa):
a) for steel; b) for concrete.

Conclusions

The use of systems protecting load-bearing structures against fire is necessary when designing steel structures. The obligation to design fire protection solutions is imposed on the designer in Poland by the Building Law.

The article presents numerical simulations of models of a steel beam in conditions simulating fire, without fire protection and for beams with various types of fire protection, mechanically loaded to the strength limit. For the purposes of calculations, it was assumed that the required fire resistance is 60 minutes, i.e. the thermal and mechanical calculation time was set at 3600 s.

In terms of thermal and mechanical load, the temperature distributions and the deformation response of the beam were analyzed for various models of fire insulation systems compared to an uninsulated beam in conditions simulating fire.

The use of fire protection systems has a significant impact on the time of safe operation of a steel structure in the event of a standard fire. The presented calculations show that the use of fire protection systems gives positive results in terms of fire protection of steel beams. From the point of view of fire protection, the most effective solution was the use of fire protection spray. Less beneficial, but still effective in comparison to the unprotected structure, were the casings made of plasterboard insulation boards and the construction of expanded clay concrete. The least beneficial solution is the construction of ordinary concrete. The use of fire protection systems affects the fire durability of the tested beam. The effect achieved is an increase in the time in which the structural element of the building should maintain its load-bearing properties in the conditions of a standard fire, thus increasing the fire resistance class.

References

[1] * * *, PN-EN 1991-1-2:2006, Eurokod 1: Oddziaływania na konstrukcje. Część 1–2: Oddziaływania ogólne. Oddziaływania na konstrukcje w warunkach pożaru.

[2] * * *, Rozporządzenie Ministra Infrastruktury z dnia 12 kwietnia 2002 r. w sprawie warunków technicznych, jakim powinny odpowiadać budynki i ich usytuowanie (DzU z 2002 r. nr 75, poz. 690 ze zm.).

[3] * * *, PN-EN 1993-1-2:2007, Eurokod 3: Projektowanie konstrukcji stalowych. Część 1–2: Reguły ogólne. Obliczanie konstrukcji z uwagi na warunki pożarowe.

[4] * * *, PN-EN 13501-1:2008 A1:2010, Klasyfikacja ogniowa wyrobów budowlanych i elementów budynków. Część 1: Klasyfikacja na podstawie wyników badań reakcji na ogień.

[5] C.P. Papadatu, D.B. Obreja, I.C. Adam-Papadatu, I.G. Sandu, *Learning from the past: The reconstruction of the original Damascus Steel. Experimental Study,* **International Journal of Conservation Science, 14**(3), 2023, pp. 871-886. DOI: 10.36868/IJCS.2023.03.07.

[6] C.P. Papadatu, D.B. Obreja, I.C. Adam-Papadatu, I.G. Sandu, *Research on Testing a Genuine Damascus Steel. A Case Study, International Journal of Conservation Science*, **International Journal of Conservation Science, 14**(4), 2023, pp.1367-1380. DOI: 10.36868/IJCS.2023.04.07.

[7] C.P. Papadatu, D.B. Obreja, I.C. Adam-Papadatu, I.G. Sandu, *Graphic Modeling and Equipment Used in the Reconstruction of the Original Damascus Steel*, **International Journal of Conservation Science, 15**(2), 2024, pp. 979-982. DOI: 10. 36868/IJCS.2024.02.15.

[8] P. Sulik, *Bierne zabezpieczenia przeciwpożarowe konstrukcji*, **Izolacje**, **3**, 2018, pp. 118–124.

[9] K. Chudyba, **Analiza konstrukcji z betonu w warunkach pożarowych**, Wydawnictwo PK, Kraków, 2019, p. 177.

[10] M. Brasseur, O. Vassart, L. Cajot, **Fire safety of industrial halls and low-rise buildings – Realistic fire design, active safety measures, post-local failure simulation and performance-based requirements**, European Commission, Directorate-General for Research and Innovation, Publications Office, 2007.

[11] * * *, **Best Practice Guide for Passive Fire Protection for Structural Steelwork, Fire Resistance and External Exposure Characteristics, the passive Fire protection Handbook I Structural steel – Corrugated steel – Concrete**, ISOVER Saint-Gobain, 2021.

[12] * * *, **The passive Fire protection Handbook I Structural steel – Corrugated steel – Concrete**, ISOVER Saint-Gobain, 2021.

[13] * * *, **The Passive Fire Protection Handbook, The UK's comprehensive guide to passive fire protection, Structural Steel**, ETE Building Performance, 2017.

[14] A. Buszko, *Ochrona przeciwpożarowa konstrukcji stalowych w budynkach magazynowych*, **Logistyka**, **4**, 2017, pp. 36-38.

[15] W. Skowroński, **Teoria bezpieczeństwa pożarowego konstrukcji metalowych**, Wydawnictwo naukowe PWN, Warszawa, 2011, p. 206.

[16] A. Biegus, *Projektowanie konstrukcji stalowych z uwagi na warunki pożarowe według Eurokodów*, **Izolacje**, **2**, 2013, pp. 20–28.

[17] A. Biegus, *Czynne i bierne zabezpieczenia ogniochronne konstrukcji stalowych*, **Izolacje**, **3**, 2013.

[18] Z. Mielczarek, **Nowoczesne konstrukcje w budownictwie ogólnym**, Arkady, Warszawa, 2005, p. 512.

[19] Y. Cao, J. Jiang, Y. Lu, W. Chen, J. Ye, *Progressive collapse of steel structures exposed to fire: A critical review*, **Journal of Constructional Steel Research**, **207**, 2023, Article Number: 107985. DOI: 10.1016/j.jcsr.2023.107985.

[20] D. Jończyk, *Methods for assessing the degree of destruction of concrete structures after a fire – review*, **Zeszyty Naukowe Politechniki Częstochowskiej**, **29**, 2023, pp. 27-31.

[21] G. Q. Li, W. Ji, Ch. Y. Feng, Y. Wang, G.B. Lou, *Experimental and numerical study on collapse modes of single span steel portal frames under fire*, **Engineering Structures**, **245**, 2021, Article Number: 112968. DOI: 10.1016/j.engstruct.2021.112968.

[22] F. Meng, N. Mago, K. Andisheh, G.C. Clifton, *Numerical validation of structural fire design for steel framed car park buildings*, **Fire Safety Journal**, 139, 2023, Article Number: 103819. DOI: 10.1016/j.firesaf.2023.103819.

[23] Y. Zhang, G. Han, Y. Wang, Z. Huang, F. Ding, Sh. Ma, H. Qi, W. Wang, G. Zhu, *Numerical analysis of the behaviour of a concrete floor in a steel-framed structure subject to a traveling fire*, **Fire Safety Journal**, **146**, 2024, Article Number: 104161. DOI: 10.1016/j.firesaf.2024.104161.

[24] M. Major, J. Nawrot, I. Major, *Structural S235 and S355 Steels – Numerical Analysis of Selected Rods Connection*, **IOP Conference Series: Materials Science and Engineering**, **585**, 2019, Article Number: 012007. DOI:10.1088/1757-899X/585/1/012007.

[25] Sh. Pang, V. Kodur, W. Wang, *Fire resistance of steel structures, incorporating HSS - review and recommendations*, **Journal of Constructional Steel Research**, **217**, 2024, Article Number: 108677. DOI: 10.1016/j.jcsr.2024.108677.

[26] X.M. Ma, J.L. Pan, J.M. Cai, Z.Y. Zhang, J.S. Han, *A review on cement-based materials used in steel structures as fireproof coating*, **Construction and Building Materials**, **315**, 2022, Article Number: 125623. DOI: 10.1016/j.conbuildmat.2021.125623.

[27] L. Laím, A. Santiago, H. Caetano, H.D. Craveiro, A. Shahbazian, *Numerical analysis and structural fire design of protected SHS steel columns with thermally enhanced gypsum-based mortars*, **Journal of Building Engineering**, **54**, 2022, Article Number: 104629. DOI: 10.1016/j.jobe.2022.104629.

[28] H.L. Nguyen, M. Kohno, *Numerical model of heat transfer for protected steel beam with cavity under ISO 834 standard fire*, **Fire Safety Journal**, **140**, 2023, Article Number: 103876. DOI: 10.1016/j.firesaf.2023.103876.

[29] M.H. Nguyen, S.E. Ouldboukhitine, S. Durif, V. Saulnier, A. Bouchair, *Passive fire protection of steel profiles using wood*, **Engineering Structures**, **275**, 2023, Article Number: 115274. DOI: 10.1016/j.engstruct.2022.115274.

[30] I. Singh, G.E. Stavroulakis, G.A. Drosopoulos, *Impact of partially damaged passive protection on the fire response of bolted steel connections using finite element analysis*, **Case Studies in Thermal Engineering**, **49**, 2023, Article Number: 103225. DOI: 10.1016/j.csite.2023.103225.

[31] P. Covi, N. Tondini, M.L. Tornaghi, F.J. Molina, P. Pegon, G. Tsionis, *Seismic experimental analysis of a full-scale steel building with passive fire protections*, **Engineering Structures**, **300**, 2024, Article Number: 117203. DOI: 10.1016/j.engstruct.2023.117203.

[32] M. Gravit, I. Dmitriev, N. Shcheglov, A. Radaev, *Oil and Gas Structures: Forecasting the Fire Resistance of Steel Structures with Fire Protection under Hydrocarbon Fire Conditions*, **Fire**, **7**(6), 2024, Article Number: 173. DOI: 10.3390/fire7060173.

[33] M. Gravit, E. Golub, B. Klementev, I. Dmitriev, *Fire Protective Glass Fiber Reinforced Concrete Plates for Steel Structures under Different Types of Fire Exposure*, **Buildings**, **11**(5), 2021. Article Number: 187. DOI: 10.3390/buildings11050187.

[34] M. Gravit, D. Shabunina, *Structural Fire Protection of Steel Structures in Arctic Conditions*, **Buildings**, **11**(11), 2021, Article Number: 499. DOI: 10.3390/buildings11110499.

[35] * * *, Aprobata Techniczna ITB nr AT-15-8163/2013 **Zaprawa mcr TECWOOL F do ogniochronnogo zabezpieczenia konstrukcji stalowych i żelbetowych**.

[36] * * *, Zaprawa ogniochronna PROMASPRAY® F250 (natrysk ogniochronny) ETA-10/0148, EC Deklaracja Zgodności 1116-CPD-0138-10/0148-21.

[37] K. Laber, M. Knapiński, H. Dyja, D. Musiał, *Doświadczalne wyznaczenie emisyjności stali S355J2G3 w zakresie temperatur 800°C-1200°C*, **Hutnik-Wiadomości Hutnicze, 76**(7), 2009, pp. 504-506.

[38] * * *, PN-EN 1992-1-2:2008, Eurokod 2: Projektowanie konstrukcji z betonu. Część 1–2: Reguły ogólne. Projektowanie z uwagi na warunki pożarowe.

[39] * * *, PN-EN ISO 10456:2009 - Materiały i wyroby budowlane. Właściwości cieplno-wilgotnościowe – Tabelaryczne wartości obliczeniowe i procedury określenia deklarowanych i obliczeniowych wartości cieplnych.

[40] M. Maślak, **Trwałość pożarowa stalowych konstrukcji prętowych**, Wydawnictwo PK, Kraków, 2008, p. 203.

[41] * * *, AS 3600-1988: Australian Standard – Concrete structures.

[42] M. Maj, T. Stachoń, A. Ubysz, *Beton jako materiał konstrukcyjny w wysokiej temperaturze*, **Materiały Budowlane**, **6**, 2014, pp. 64-65.

[43] Z. Bednarek, R. Krzywobłocka-Laurów, T. Drzymała, *Wpływ wysokiej temperatury na strukturę, skład fazowy i wytrzymałość betonu*, **Zeszyty Naukowe SGSP**, **38**, 2009. pp. 6 – 26.

[44] * * *, ANSYS Inc. (2021). Material Reference, Canonsburg, USA.

[45] P. Menetrey, K. J. Willam, *Triaxial failure criterion for concrete and its generalization*, **ACI Structural Journal**, **92:3**, 1995, pp. 311-318.

[46] * * *, PN-H-93419:1997+Ap1:2002 – DIN1025 Teil 5:1994 – Euronorm 19-57.

[47] * * *, EN 10034:1993 – PN-EN 10034:1996+Ap1:1999.
[48] * * *, PN-EN 1990:2004 Eurokod 0: Postawy projektowania konstrukcji.

Received: June 20, 2024
Accepted: November 28, 2024

.